

Production of Gravitational Waves in the nMSSM

Stephan J. Huber⁽¹⁾ and Thomas Konstandin^{(2)*}

(1) *Department of Physics and Astronomy,*

University of Sussex, Brighton, BN1 9QJ, UK and

(2) *Department of Theoretical Physics,*

Royal Institute of Technology (KTH), AlbaNova University Center,

Roslagstullsbacken 21, 106 91 Stockholm, Sweden

(Dated: January 13, 2019)

During a strongly first-order phase transition gravitational waves are produced by bubble collisions and turbulent plasma motion. We analyze the relevant characteristics of the electroweak phase transition in the nMSSM to determine the generated gravitational wave signal. Additionally, we comment on correlations between the production of gravitational waves and baryogenesis. We conclude that the gravitational wave relic density in this model is generically too small to be detected in the near future by the LISA experiment. We also consider the case of a "Standard Model" with dimension-six Higgs potential, which leads to a slightly stronger signal of gravitational waves.

I. INTRODUCTION

Presently, several experiments are under consideration that could detect for the first time a stochastic background of gravitational waves (GWs). One of the main motivations to pursue these experiments is that the discovery of a relic gravitational background would be a smoking gun signal from inflation [1] and hence might allow to test the paradigm of an era of exponential expansion in the early Universe.

Another source of stochastic GWs are strongly first-order phase transitions. Space-based experiments, such as LISA [2] and BBO [3] will have remarkably good sensitivity at frequencies that coincide with the redshifted spectrum of GWs produced during an electroweak

*s.huber@sussex.ac.uk; konstand@kth.se

phase transition at temperatures $T \sim 100$ GeV. This opens the possibility to infer information about the electroweak phase transition from GW observations. A strongly first-order phase transition not only would produce GWs, but could also generate the observed baryon asymmetry of the Universe (BAU) through electroweak baryogenesis [4, 5]. This way the observation of a stochastic background of GWs might teach us about electroweak baryogenesis in extensions of the Standard Model (SM).

During a first-order phase transition there are two distinct mechanisms that produce GWs: The colliding phase boundaries [6, 7, 8, 9], and the turbulent motion of the plasma [10, 11, 12, 13, 14]. Concerning the latter, there is an ongoing discussion in the literature on how to correctly model the temporal correlation of the turbulent plasma. In particular, the different approaches predict different peak frequencies of the resulting GW spectrum.

Studies of GWs from the electroweak phase transition have been performed in Refs. [15] and [16] without relying on particular particle physics models. The results are presented as functions of the two main parameters of the problem, which are the typical size of the colliding bubbles and the available energy. It was concluded that a sufficiently strong phase transition could lead to an observable GW signal at LISA. Of course, in a given model the bubble size and the available energy are linked, and it is interesting to see what happens to the GW signal. The cases of the MSSM and the NMSSM (Next-to-minimal supersymmetric SM) were studied in Ref. [17]. While it was found that in the MSSM the produced amount of GWs is orders of magnitude below the LISA sensitivity, the situation in the NMSSM seems much more promising. The cubic terms present in the NMSSM tree-level Higgs potential can lead to a much stronger phase transition [18].

However, the authors of Ref. [17] used a crude method to determine the bubble configurations, which overestimates the strength of the phase transition and the GW signal. The aim of this work is to improve on this point to arrive at a more realistic estimate of the signal strength. To achieve this we apply our recently presented numerical method to compute the bubble shapes [19].

Like in Ref. [17] we consider a singlet extension of the MSSM, in our case the nearly Minimal Supersymmetric Standard Model (nMSSM) [20]. In contrast to the models studied in Refs. [17, 18], it solves the μ -problem of the MSSM, without creating a domain wall problem or destabilizing the electroweak hierarchy through divergences of the singlet tadpole. With this motivation, the cosmology of the nMSSM has been studied intensively in

the literature. It was shown in Ref. [21] that the model can have a strong enough phase transition for baryogenesis, while the lightest neutralino can at the same time provide the dark matter of the Universe. The baryon production was studied with a positive result recently in Ref. [22]. Finally, Ref. [23] investigated to what extent these cosmological issues can be studied at colliders, in particular at the LHC.

In this paper, we compute the GW signal in the nMSSM using numerically determined bubble configurations. In addition, correlations between the amount of the produced GWs and the generated BAU are discussed. Our results for GW production are less optimistic than the estimates of Ref. [17], making it doubtful for LISA to detect a GW signal, even for an optimal choice of parameters. BBO, on the other hand, could detect GWs if the nMSSM phase transition is extremely strong. This study is a continuation of work on the baryon asymmetry in the nMSSM that has been published recently in Ref. [22]. Since the formalism to determine the BAU, the analysis of the phase transition and phenomenological aspects of the nMSSM are discussed in detail in Refs. [21, 22], we will be rather brief on these issues. We also study GW production in the SM augmented by dimension-six operators. Such a model can be viewed as the effective low energy description of some strongly coupled dynamics at the TeV scale. As this model has only one Higgs field and few parameters, the analysis is much simplified and more transparent compared to the nMSSM case. It has been shown that an H^6 -term in the Higgs potential easily leads to a strong phase transition [24, 25, 26]. Additional dimension-six operators can also provide new sources of CP violation that can account for the observed baryon asymmetry [26, 27] without generating large electric dipole moments [28].

The paper is organized as follows. The next section contains the formalism to determine the relevant properties of the phase transition. In Sec. III the H^6 model is discussed, while in Sec. IV the nMSSM and its temperature dependent effective potential is summarized. In Sec. V the numerical results for the nMSSM are presented before we conclude in Sec. VII. Appendix A contains a brief review of first-order phase transitions in cosmology.

II. GRAVITATIONAL WAVES

The discussion of GW production in this section closely follows the analysis in Ref. [15]. Details about the GW production during a first-order phase transition can be found in this

work and the references therein.

One source of GWs during the phase transition results from colliding Higgs bubbles at the end of the phase transition. Depending on the strength of the phase transition, the bubble wall profile propagates faster or slower than the speed of sound, which is $1/\sqrt{3}$ in a relativistic thermal bath. In the former case GWs are produced by *detonation*, while in the latter case *deflagration* is the dominating process. Since GW production is strongly suppressed in a deflagration, we focus in the following on the detonation mode as discussed in Refs. [6, 7, 8, 9, 29].

To determine the magnitude of the produced GWs, two parameters of the phase transition are essential. The first one is related to the latent heat,

$$\epsilon_* = -\Delta V + T_* \left. \frac{\partial V}{\partial T} \right|_{T_*}, \quad (1)$$

which provides the energy available to be transferred to GWs. The amount of GWs depends on the ratio of the latent heat to the energy density of the radiation in the plasma,

$$\alpha = \frac{30\epsilon_*}{\pi^2 g_* T_*^4}. \quad (2)$$

This parameter measures the strength of the phase transition, as relevant for the GW production. T_* denotes the temperature of the phase transition, and g_* is the effective number of degrees of freedom (in the SM: $g_* = 107.75$). There are several prescriptions to define the start and end of the phase transition, and the time of maximal GW production. This temperature is further specified in the Appendix, see Eq. (A10).

The second parameter that enters the production of GWs is the typical radius of the colliding bubbles, $\langle R \rangle$. It sets the length scale of the problem. It can roughly be expressed as the product of the wall velocity, v_b , and the duration of the phase transition, τ . The latter can be approximately related to the logarithmic time derivative, β , of the nucleation rate, $\tau \approx \beta^{-1}$. In adiabatic approximation one has

$$\frac{\beta}{H_*} = -T_* \frac{d}{dT} \left(\frac{S_3}{T} \right) \Big|_{T_*}, \quad (3)$$

where H_* denotes the Hubble parameter at T_* . Hence, the typical length scale is proportional to

$$\langle R \rangle \propto v_b \tau \approx \frac{v_b}{\beta}. \quad (4)$$

In contrast to Ref. [17], we state our results in terms of the typical radius of the detonating bubbles $\langle R \rangle$ instead of using the approximate expression containing β . It is not known what is the optimal definition for $\langle R \rangle$. Following Ref. [15], we use the maximum of the bubble volume distribution, which should be closely related to the typical scale for energy injection into the turbulent plasma. In this case, one obtains

$$\langle R \rangle \approx 3 \frac{v_b}{\beta}. \quad (5)$$

The relevant formulas can be found in the Appendix.

The energy density in GWs per logarithmic unit of frequency is usually normalized to the critical density,

$$\Omega(f) = \frac{1}{\rho_{\text{crit}}} \frac{d\rho_{\text{GW}}(f)}{d \ln f}. \quad (6)$$

The GW contribution from colliding bubbles at the peak frequency, as observed today, is then given by [9]

$$h_0^2 \Omega_{\text{det}} \simeq 1.2 \times 10^{-7} \kappa^2 \langle R \rangle^2 H_*^2 \left[\frac{\alpha}{\alpha + 1} \right]^2 \left[\frac{v_b^2}{0.24 + v_b^3} \right]^2 \left[\frac{100}{g_*} \right]^{1/3}. \quad (7)$$

Assuming a detonation, i.e. a strong phase transition with a supersonic bubble wall, the wall velocity v_b is approximately given by [29]

$$v_b(\alpha) = \frac{1/\sqrt{3} + \sqrt{\alpha^2 + 2\alpha/3}}{1 + \alpha}. \quad (8)$$

This is a good approximation for very strong phase transitions. Finally, the efficiency κ is [9]

$$\kappa(\alpha) \simeq \frac{1}{1 + 0.715\alpha} \left[0.715\alpha + \frac{4}{27} \sqrt{\frac{3\alpha}{2}} \right]. \quad (9)$$

It measures the fraction of latent heat that is transformed into bulk motion of the fluid.

The second source of GWs during the phase transition is turbulence [9, 10, 12]. When the bubbles collide, the plasma is stirred up, which creates a cascade of eddies in the plasma. The relic GW density at the peak frequency coming from turbulence, according to Refs. [12, 15], is found to be

$$h_0^2 \Omega_{\text{turb}} \simeq 5.6 \times 10^{-6} u_S^5 \langle R \rangle^2 H_*^2 \left[\frac{100}{g_*} \right]^{1/3}. \quad (10)$$

As additional parameter, the characteristic turnover velocity u_S of the eddies in the plasma enters, given by [15]

$$u_S \simeq \sqrt{\frac{\kappa\alpha}{4/3 + \kappa\alpha}}. \quad (11)$$

The expression (10) relies on a certain modeling of time correlations in the turbulence, which was introduced in Ref. [11]. Similar results were obtained using Kraichnan's ansatz for the time correlations [14].

Recently, a different approach in calculating the contribution from turbulence was presented in Ref. [13]. This work is based on Richardson's model of turbulent motion which is based on random velocities of the turbulent fluid. The authors of Ref. [13] emphasize the fact that the GWs inherit the momentum spectrum from the eddies rather than their frequency spectrum. The resulting GW density at the peak frequency is

$$h_0^2 \Omega_{\text{Richardson}} \simeq 6.7 \times 10^{-6} u_S^4 \langle R \rangle^2 H_*^2 \left[\frac{100}{g_*} \right]^{1/3}. \quad (12)$$

Notice that one reason for the different results of the two approaches to turbulence in terms of β lies in the fact that in Ref. [13] the typical bubble radius is given by $\langle R \rangle \approx v_b/\beta$, while in Ref. [12] the relation $\langle R \rangle \approx 5 v_b/\beta$ was used. Our choice of Eq. (5) lies in between these two cases. Deciding between these different approaches to turbulence is beyond the scope of the current paper. We simply present results for both cases, indicating the spread in the theoretical predictions.

For weaker phase transitions the contributions from bubble collisions are larger than the ones from turbulence, but if the phase transition is really strong, $u_S \sim v_b$, both contributions can be of comparable magnitude or the latter can even dominate.

Since we assume the phase transition to lead to supersonic bubble wall expansion and use the GW production formula at the frequency peak, the given production rates of GWs should be understood as upper bounds. If the wall velocity is subsonic, detonation does not take place and the contribution of turbulence is strongly reduced, not only because the velocity v_b is small, but also because the efficiency factor κ is much smaller than in Eq. (9), which as well assumes supersonic bubble velocities.

To roughly determine the spectrum of the GWs, it is sufficient to know the peak frequency and the scaling behavior. The peak frequencies are given by

$$f_{\text{det}} \simeq 1.6 \times 10^{-2} \text{mHz } v_b \frac{1}{\langle R \rangle H_*} \frac{T_*}{100 \text{ GeV}} \left[\frac{g_*}{100} \right]^{1/6}, \quad (13)$$

$$f_{\text{turb}} \simeq 1.7 \times 10^{-2} \text{mHz } u_S \frac{1}{\langle R \rangle H_*} \frac{T_*}{100 \text{ GeV}} \left[\frac{g_*}{100} \right]^{1/6}, \quad (14)$$

$$f_{\text{Richardson}} \simeq 1.7 \times 10^{-2} \text{mHz } \frac{1}{\langle R \rangle H_*} \frac{T_*}{100 \text{ GeV}} \left[\frac{g_*}{100} \right]^{1/6}. \quad (15)$$

Notice that the peak frequency in Richardson's model differs from the "usual" result for a turbulent plasma by a factor u_S due to the dispersion relation of the eddies. This shifts the peak frequency to higher values. This fact is relevant observationally, as the peak frequencies for GWs from the electroweak phase transition are typically at the lower end of the LISA window, where its sensitivity is already reduced.

The GW spectrum from bubble collisions rises as $f^{2.8}$ below and decreases as $f^{-1.8}$ above the peak. The corresponding scaling behavior in the case of turbulence is given by $f^{2.0}$ and $f^{-3.5}$, respectively. Finally, the scaling behavior in the analysis based on Richardson's model is given by

$$h_0^2 \Omega_{\text{Richardson}} \propto \begin{cases} f^3, & f < 2u_S f_{\text{peak}} \\ f, & 2u_S f_{\text{peak}} < f < f_{\text{peak}} \\ f^{-8/3}, & f_{\text{peak}} < f \end{cases}. \quad (16)$$

III. THE STANDARD MODEL WITH DIMENSION-SIX OPERATORS

Before turning to the nMSSM, let us discuss GW production in a simple "toy model". It consists of the SM augmented by certain dimension-six operators. These operators parametrize unknown physics at the cutoff scale, typically at a few hundred GeV. They could originate from some new strong dynamics, such as technicolor or weak scale gravity, or from simply integrating out scalar fields.

The model contains a single Higgs doublet, H , whose potential is stabilized by an H^6 interaction [24, 25, 26]

$$V(H) = -\frac{\mu^2}{2}H^2 + \frac{\lambda}{4}H^4 + \frac{1}{8M^2}H^6. \quad (17)$$

This potential has two free parameters, the suppression scale of the dimension-six operator, M , and the quartic coupling, λ . The latter can be eliminated in terms of the physical Higgs mass, m_H . Since the potential is stabilized by the H^6 term, λ can be negative. In this case a barrier in the Higgs potential is present at tree-level, which induces a strong first-order electroweak phase transition. Evaluating the one-loop thermal potential, it was shown in Ref. [26] that the phase transition is strong enough to avoid baryon number washout, i.e. $\langle H \rangle_{T_c}/T_c > 1.1$ [30], if $M < 850$ GeV and $m_H = 115$ GeV. At the critical temperature, T_c , the broken and symmetric phases are degenerate in energy. Taking $M = 500$ GeV, a strong phase transition is present for $m_H < 180$ GeV.

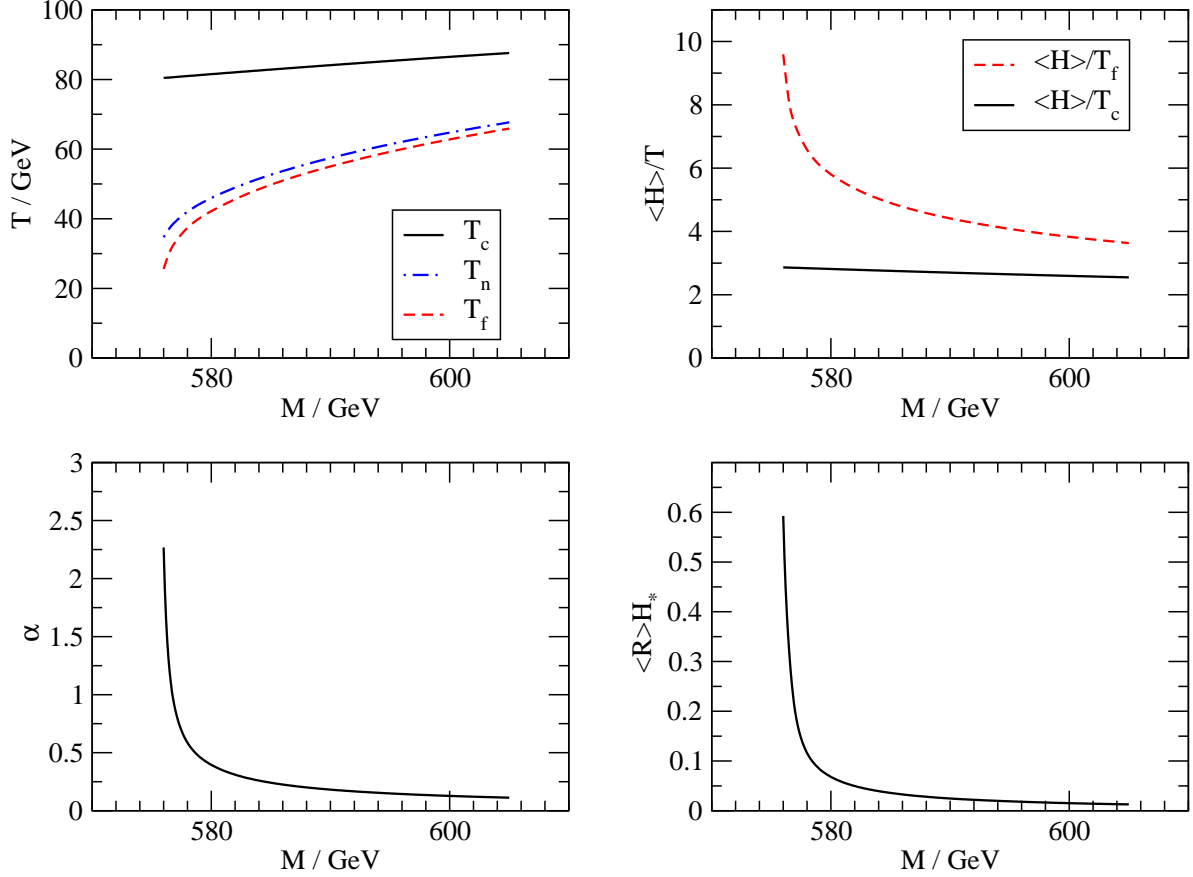


FIG. 1: Different characteristics of the phase transition as functions of the parameter M .

Dimension-six operators also induce new sources of CP violation. In addition to the ordinary Yukawa interaction of the top quark, $y_t H t^c q_3$, one has an operator $(x_t/M^2)(H^\dagger H) H t^c q_3$. Along the bubble wall these two contributions to the top quark mass enter with varying weight. In this way a possible relative phase between the two operators induces a varying complex phase in the top quark mass such that tops and anti-tops behave differently in the bubble background. Chiral charges are built up in front of the bubble wall, which the sphalerons transform into a baryon asymmetry. A semi-classical analysis of these processes has been performed in Refs. [26, 27]. It was shown that the observed BAU can indeed be produced this way. This can be achieved without generating dangerously large electric dipole moments [28].

To compute the spectrum of GWs one has to study the real time history of the electroweak phase transition, in particular one must determine the parameters α and $\langle R \rangle$. This requires knowledge of the bubble nucleation rate, which depends on the energy of the nucleating

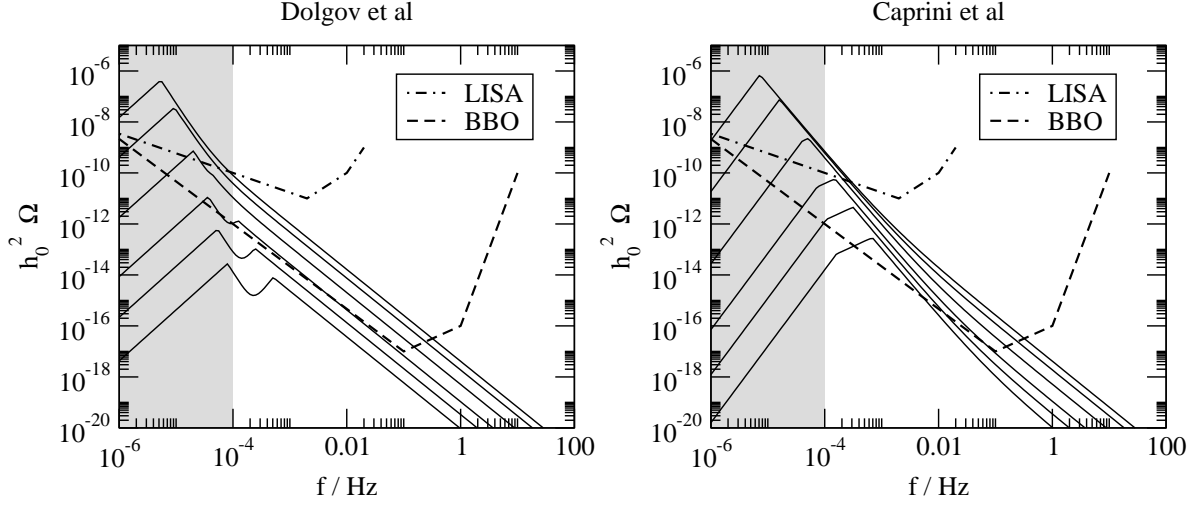


FIG. 2: The spectrum of the density of GWs for different values of the parameter M . The used parameters are given in Tab. I.

bubbles and varies with temperature. The bubble configuration is a stationary solution to the Euclidean equations of motion of the Higgs fields. The relevant formulas are collected in the Appendix. We use the one-loop thermal Higgs potential as described in Ref. [26]. Since there is only one Higgs field, the bubble solution can be obtained by a simple over/under-shooting method.

We define the onset of the phase transition as the temperature, T_n , where the first bubble per horizon volume nucleates, (A7). As the Universe cools down more bubbles nucleate, expand and finally collide. During this stage one can neglect the expansion of the Universe, which should only matter for extremely strong phase transitions, $\beta \approx H_*$. Most bubbles collide at the end of the phase transition, which can be defined as the temperature, T_f where a fraction of $1 - 1/e = 0.632$ of the volume is converted into the broken phase, (A10). Finally, we obtain $\langle R \rangle$ from the maximum of the bubble volume distribution at T_f , as mentioned before.

In our numerical example we use the Higgs mass $m_H = 120$. We have checked that for larger Higgs masses the results are essentially the same, only the relevant values of M change. When M decreases, the strength of the phase transition increases. At $M \sim 576$ GeV the system becomes metastable and the Universe gets stuck in the symmetric phase. As shown in Fig. 1 the phase transition is strong enough to avoid washout after electroweak

| set | M / GeV | α | $\langle R \rangle H_*$ | T_* / GeV |
|-----|-----------|----------|-------------------------|-------------|
| 1 | 600.0 | 0.128 | 0.015 | 62.8 |
| 2 | 588.0 | 0.201 | 0.028 | 53.1 |
| 3 | 582.0 | 0.311 | 0.050 | 45.6 |
| 4 | 578.0 | 0.586 | 0.116 | 37.4 |
| 5 | 576.5 | 1.197 | 0.318 | 30.4 |
| 6 | 576.0 | 2.268 | 0.592 | 25.6 |

TABLE I: Sets of parameters used in Fig. 2.

baryogenesis. While T_c and $\langle H \rangle / T_c$ change only slowly in the presented range of M , T_f and T_n drop rapidly. This signals that the system is close to metastability. At the same time α rises from a value around 0.1 to order unity and the typical bubble radius $\langle R \rangle$ increases dramatically. In Fig. 2 the GW spectrum for several choices of M is shown, as given in Tab. I, together with the LISA and BBO sensitivities. In gray the region of $f < 10^{-4}$ Hz is indicated, where observational sensitivities drop considerably. The plot demonstrates that as the phase transition becomes stronger and the amplitude of the GW signal becomes larger, the peak frequency moves to lower values. This is directly related to the smaller values T_f and larger values of $\langle R \rangle H_*$ in Fig. 1. As a result, even in the case of an extremely strong transition, $M \sim 576$ GeV, it will be difficult for LISA to detect a GW signal. This would require sensitivity at lower frequencies. Things are different for BBO. It would be able to detect GWs if $M < 585$ GeV, which corresponds to a few percent tuning in M . In this case also the subtraction of backgrounds, in particular from white dwarf binaries, has to be under control (see [16], and references therein). The main difference between the two models of turbulence is that in the case of the Richardson model the two-peak structure in the GW spectrum disappears, as the turbulence contribution is shifted to higher frequencies. If present and observed, the double-peak structure could help to identify a phase transition as source of the GW signal. Comparing with the general analysis in Ref. [16] we arrive at a more pessimistic picture because large values of α mean small $\langle R \rangle$ and a low peak frequency. The decrease in temperature for very strong phase transitions additionally enhances this effect.

IV. THE NMSSM

While the electroweak phase transition in the MSSM is too weak to produce observable GWs [17], the strength of the phase transition increases considerably if the MSSM is equipped with an additional gauge singlet [18]. There are various possibilities to implement this idea. A phenomenologically attractive candidate is the nMSSM [20] with the superpotential

$$W_{\text{nMSSM}} = \lambda \hat{S} \hat{H}_1 \cdot \hat{H}_2 - \frac{m_{12}^2}{\lambda} \hat{S} + W_{\text{MSSM}}. \quad (18)$$

In contrast to the models studied in Ref. [18], it solves the μ -problem of the MSSM without destabilizing the electroweak hierarchy or the generation of domain walls at the electroweak phase transition. However, the discrete R-symmetry necessary to accomplish this task, forbids the singlet self-coupling and leads to a quite constrained Higgs and neutralino/chargino phenomenology [21, 22]. For instance, the singlino obtains its mass only by mixing with the Higgsinos. It is typically very light, and can be a dark matter candidate [21].

The tree-level Higgs potential of the nMSSM including soft SUSY breaking terms reads

$$V = V_F + V_D + V_{\text{soft}}, \quad (19)$$

where

$$\begin{aligned} V_F &= m_1^2 H_1^\dagger H_1 + m_2^2 H_2^\dagger H_2 + m_s^2 |S|^2 \\ &\quad + \lambda^2 |H_1 \cdot H_2|^2 + \lambda^2 |S|^2 (H_1^\dagger H_1 + H_2^\dagger H_2), \\ V_D &= \frac{g^2 + (g')^2}{8} (H_2^\dagger H_2 - H_1^\dagger H_1)^2 + \frac{g^2}{2} |H_1^\dagger H_2|^2, \\ V_{\text{soft}} &= t_s (S + h.c.) + (a_\lambda S H_1 \cdot H_2 + h.c.), \\ &\quad - m_{12}^2 (H_1 \cdot H_2 + h.c.). \end{aligned} \quad (20)$$

Additionally, we take into account the Coleman–Weinberg one-loop terms

$$\Delta V = \frac{1}{16\pi^2} \left[\sum_b g_b h(m_b^2) - \sum_f g_f h(m_f^2) \right], \quad (21)$$

where the two sums run over bosons and fermions with the degrees of freedom g_b and g_f respectively, and

$$h(m^2) = \frac{m^4}{4} \left[\ln \left(\frac{m^2}{Q^2} \right) - \frac{3}{2} \right]. \quad (22)$$

At finite temperature, the effective potential is modified by the following thermal one-loop contributions:

$$\Delta V^T = \frac{T^4}{2\pi^2} \left[\sum_b g_b J_+(m_b^2/T^2) - \sum_f g_f J_-(m_f^2/T^2) \right], \quad (23)$$

with

$$J_{\pm}(y^2) = \int_0^\infty dx x^2 \log(1 \mp \exp(-\sqrt{x^2 + y^2})). \quad (24)$$

For both one-loop contributions we use the following numbers of degrees of freedom

$$g_W = 6, \quad g_Z = 3, \quad g_t = 12, \quad g_{\tilde{t}_1} = g_{\tilde{t}_2} = 6, \quad (25)$$

and the renormalization scale is chosen to be $Q = 150$ GeV. As most SUSY particles are assumed to be heavy, we approximate the number of effective degrees of freedom by the SM value, $g_* = 107.75$.

At zero temperature, both Higgs fields and the singlet field acquire a vev and the Higgs vevs are constrained by

$$\phi(T=0) = v \simeq 174 \text{ GeV}, \quad \phi^2(T) = |\langle H_1^0 \rangle_T|^2 + |\langle H_2^0 \rangle_T|^2. \quad (26)$$

Additionally, since one of the chargino masses is approximately given by

$$m_{\chi^\pm} \approx \lambda \langle S \rangle \gtrsim 114 \text{ GeV}, \quad (27)$$

the parameter space is restricted to regions with a sufficiently large singlet vev. The lower bounds on the masses of the physical Higgs states further restrict the parameter space, such that the nMSSM constitutes a much stronger constrained model than models with an explicit Higgsino/chargino mass (μ -term) or a singlet self-coupling. These bounds are easier to satisfy for larger values of λ , which therefore prefers to be close (even beyond) the Landau pole value.

V. NUMERICAL ANALYSIS

Our numerical analysis follows the approach already used in Ref. [22] to determine the BAU in the nMSSM. The relevant eight free parameters of the nMSSM are chosen randomly. The generated parameter sets are then confronted with several constraints on the mass

spectrum and the Z-width (for details see Ref. [22]). In addition, we restrict ourselves to cases which promise a rather strong phase transition, $\phi(T_c)/T_c \gtrsim 1$, by inspection of the potential. If the parameter set passes these constraints, the properties of the phase transition and the GW relic density are determined.

Compared to the former work on the GW production in the NMSSM [17], the analysis is improved in the following points. First, we use up-to-date bounds on the particle spectrum, which severely constrains the parameter space. Second, the bubble configurations of the six scalar fields are determined exactly, while in Ref. [17] this problem was reduced effectively to a one-dimensional one, which overestimates the strength of the phase transition and hence the GW production. Third, the parameters relevant for baryogenesis are determined in the specific cases and hence a direct correlation between the BAU and the magnitude of the GWs can be inferred.

Because of the linear and tri-linear terms of the singlet in the potential (20), a strongly first-order phase transition in the nMSSM is possible due to tree-level dynamics [21, 22, 31, 32]. The phase transition in this case is described by six fields: The two vevs of the neutral Higgs fields $\langle H_1^0 \rangle$, $\langle H_2^0 \rangle$, the vev of the singlet $\langle S \rangle$ and their complex phases; however, the relative phase between the Higgs vevs does not enter the potential and can be removed using its equation of motion. In this work, the profiles of the vevs during the phase transition are calculated numerically using the method presented in Ref. [19] that is briefly described in Appendix A.

The left panel of fig. 3 shows the correlation between the parameters α , the available energy, and $\langle R \rangle H_*$ for approximately 150 parameter sets. We find the same behavior as in the SM with dimension-six operators. The right panel compares the typical bubble size with β at first nucleation, $T = T_n$, and the end of the phase transition, $T = T_f$. Note that $\beta(T_n)$ usually underestimates the bubble radius, while $\beta(T_f)$ overestimates it. For strong phase transitions, β varies considerably between T_n and T_f . This makes our more careful determination of $\langle R \rangle$ necessary. The same applies to the SM with dimension-six operators.

Since there is a relatively strong correlation between α and the bubble radius, we correlate in the following only the parameter α with the parameters that enter the determination of the BAU and the production of GWs.

Figure 4 shows several characteristic properties of the phase transition. In all parameter sets under consideration, baryon number washout after the phase transition is sufficiently

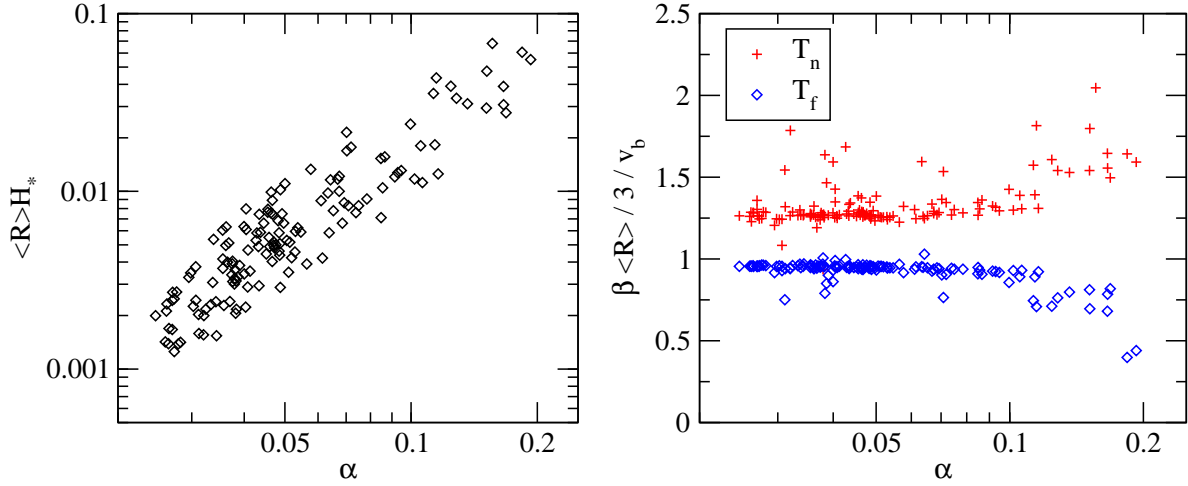


FIG. 3: The left panel shows the correlation between the parameters α and the typical size of the bubbles at the end of the phase transition, $\langle R \rangle$. The right panel compares the typical bubble size with β at first nucleation, $T = T_n$, and the end of the phase transition, $T = T_f$.

suppressed [30], $\phi(T_f)/T_f \gtrsim 1.1$. As concluded in Ref. [22], electroweak baryogenesis is a generic feature for this class of models. However, this statement is based on the assumption that the wall velocity is subsonic, such that diffusion is operative. From the parameters that enter the generation of the BAU in Eq. (35), three are expected to have a strong dependence on the strength of the phase transition: The wall thickness l_w and the temperatures T_n and T_f . These quantities are also plotted against the parameter α in Fig. 4. Both, the wall thickness and the temperatures, decrease with increasing strength of the phase transition.

The magnitude of the produced gravitational waves is displayed in Fig. 5, separately for the contribution from collisions and turbulence. For our parameter sets, the strength of the phase transition never exceeds $\alpha = 0.2$ and the density of the produced GWs is too low to be observed by the LISA experiment that has a sensitivity of $h_0^2 \Omega \sim 10^{-11}$. On the other hand, the BBO experiment has a maximal sensitivity of $h_0^2 \Omega \sim 10^{-17}$ which is several orders below the maximal GW density we found, $h_0^2 \Omega \sim 10^{-11}$.

However, even the prospects for the BBO experiment to observe GWs from a strongly first-order phase transition in the nMSSM are very limited as seen in Fig. 6. The plot shows six spectra corresponding to the parameters given in Table II. Even for relatively strong phase transitions, the spectrum of GWs would escape detection, since a stronger phase transition proceeds at lower temperatures and leads to larger bubbles, as can be seen

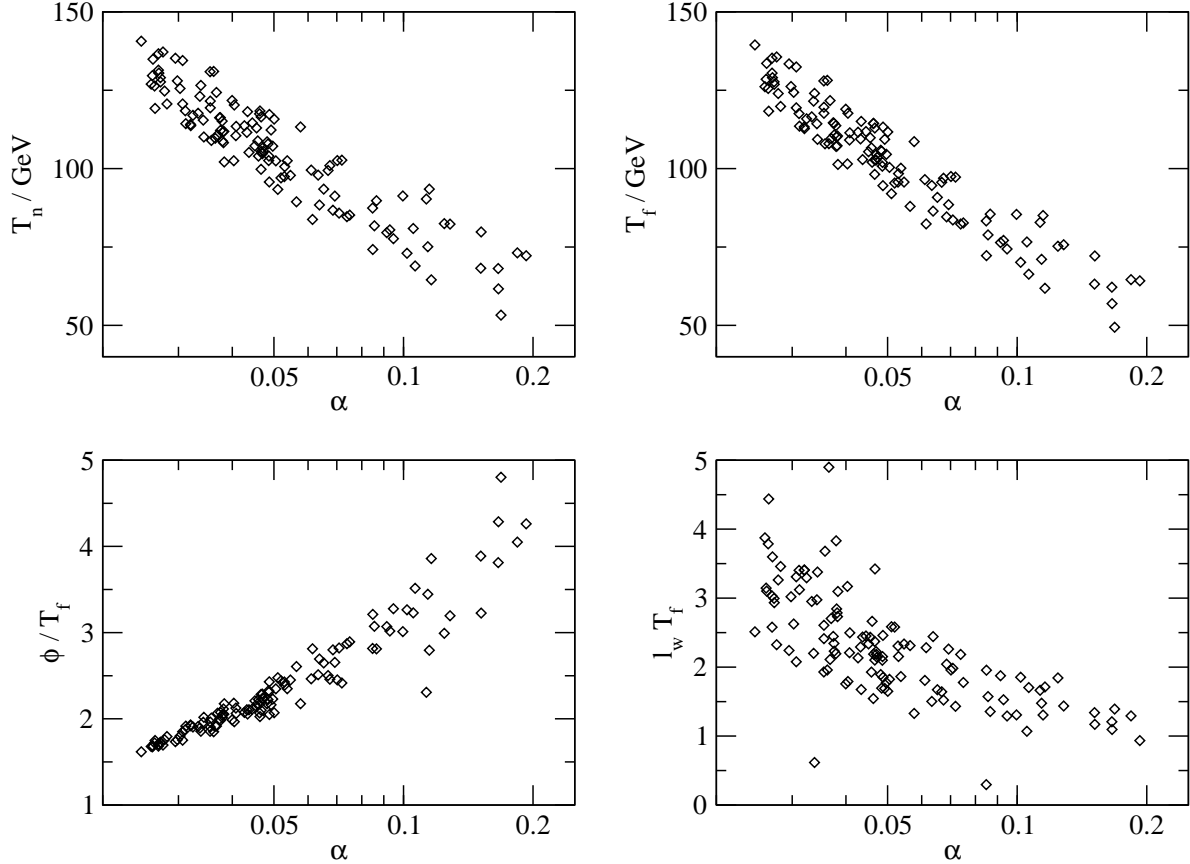


FIG. 4: The correlation between the parameter α and several properties of the phase transition: The temperature at first nucleation T_n , the temperature at the end of the phase transition T_f , the thickness of the bubble wall l_w and the ratio between the Higgs vev and the temperature $\phi(T_f)/T_f$.

in Fig. 4. This effect lowers the peak frequencies according to Eqs. (13) to regions where the sensitivity of BBO is strongly reduced. This is the same phenomenon we already observed in the SM with dimension-six operators.

This leaves the question why the nMSSM does not seem to have a region in parameter space where α is very large, as observed in the NMSSM in Ref. [17]. One might think that the nMSSM is much more constrained than the NMSSM and that Higgs and chargino masses in accordance with current LEP bounds strongly restrict the parameter space of viable models. Nevertheless, the nMSSM admits very strong phase transitions induced by tree-level terms, even leading to metastability. So the crucial difference seems to be that we determine the tunnel action exactly, while in the work [17] the problem was reduced to one dimension, which can considerably overestimate the strength of the phase transition.

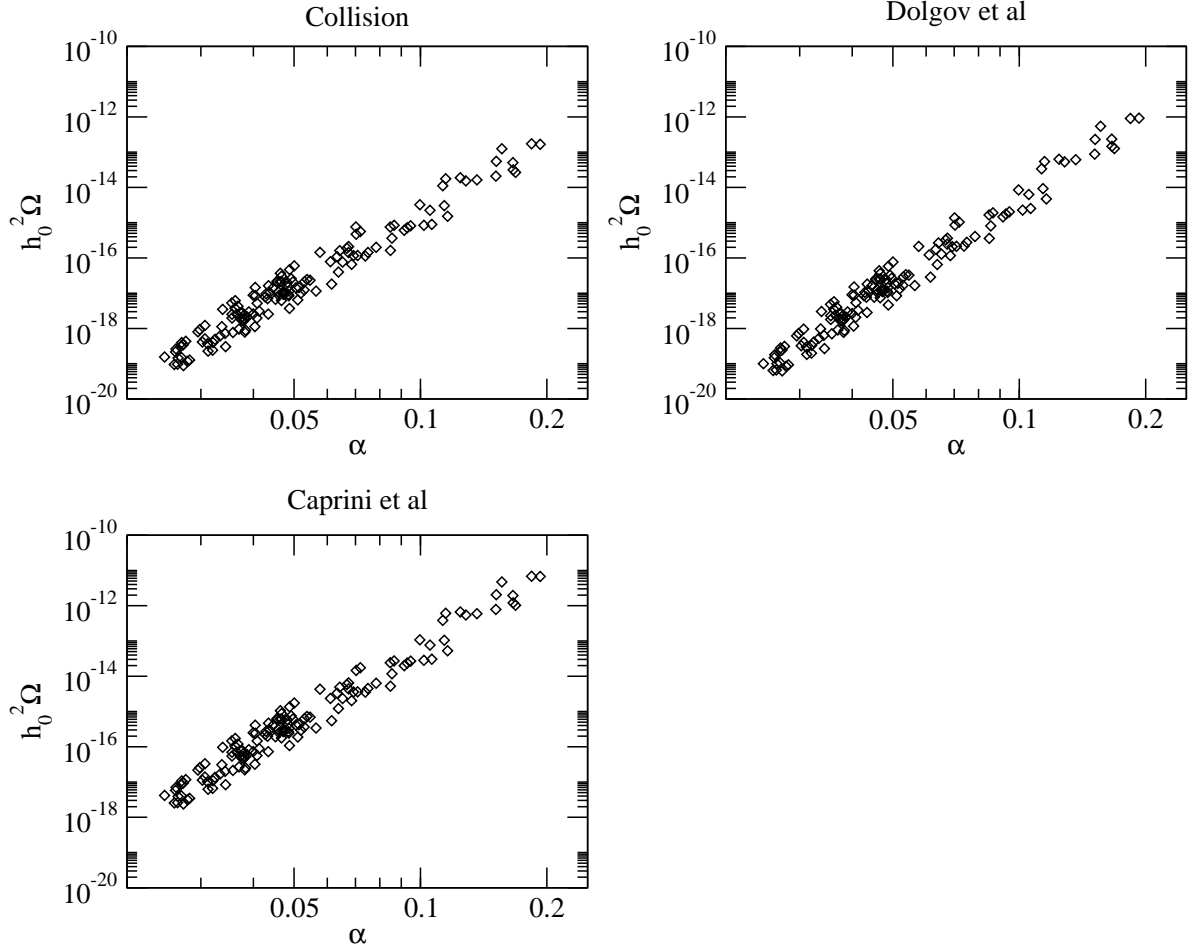


FIG. 5: The magnitude of the produced gravitational waves for our set of models. The panels show the GWs from collisions and from turbulence following the two different approaches under consideration.

According to Eq. (2), large α requires either large amounts of latent heat or small nucleation temperatures. The latent heat cannot be made arbitrarily large. For example, very small/large values for a_λ or t_s can lead to an unbounded effective one-loop potential or are not compatible with the mass constraints (one explicit example is given in Ref. [22]). Thus, the upper bound of the latent heat is expected to be limited approximately by the electroweak scale ($v \simeq 174$ GeV) and stronger phase transitions require smaller temperatures

$$\alpha \lesssim \mathcal{O}\left(\frac{30}{\pi^2 g_*} \frac{v^4}{T_*^4}\right). \quad (28)$$

On the other hand, the nucleation temperature T_* cannot be many orders smaller than the temperature T_c , where the two minima of the effective potential are degenerate. This can

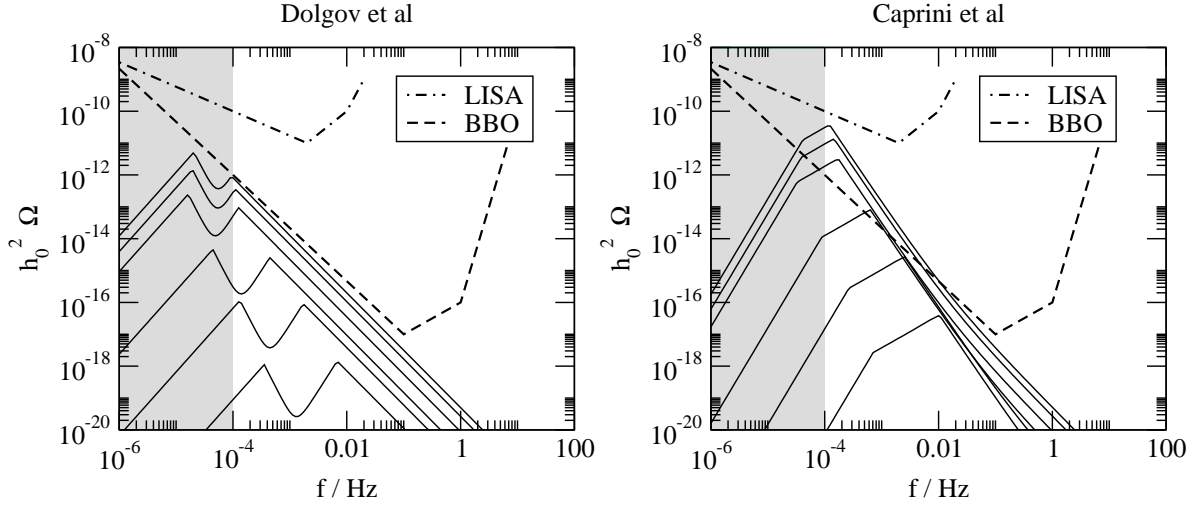


FIG. 6: The spectrum of the density of GWs for different nMSSM models. The used parameters are given in Tab. II.

| set | α | $\langle R \rangle H_*$ | T_* / GeV |
|-----|----------|-------------------------|--------------------|
| 1 | 0.03 | 0.003 | 130 |
| 2 | 0.05 | 0.01 | 110 |
| 3 | 0.07 | 0.03 | 85 |
| 4 | 0.1 | 0.1 | 80 |
| 5 | 0.15 | 0.1 | 70 |
| 6 | 0.2 | 0.1 | 60 |

TABLE II: Sets of parameters used in Fig. 6.

be seen in the following way. Assume that the Higgs vev is close to its zero temperature value, $\phi(T) \approx v$, and that the potential is of the form

$$\Delta V(T) = \Delta V(0) + \tilde{g}^2 T^2 v^2 = \tilde{g}^2 (T^2 - T_c^2) v^2, \quad (29)$$

with some constant \tilde{g} that mostly depends on the particle content of the theory. Since the three-dimensional action S_3 scales as ΔV^{-2} for small ΔV , the condition in Eq. (A13) turns into

$$\left. \frac{S_3(T)}{T} \right|_{T_*} = \frac{S_3(0)}{T_*} \frac{T_c^4}{(T_c^2 - T_*^2)^2} \approx 140. \quad (30)$$

This implies $T_* > \frac{1}{5}T_c$, since the critical temperature has to be larger than the minimum

of this function. The numerical results in the nMSSM show that the minimum is rather given by $T_* > cT_c$ with the constant $c \approx 0.5$. This is mainly due to the fact that the three-dimensional action only scales as ΔV^{-2} for very small ΔV . The closer T_* is to the minimum, the larger is α and the smaller is β . This in turn leads to the fact that small critical temperatures require small latent heat, since one obtains, using Eq. (29),

$$|\Delta V(0)| < \epsilon_* = \tilde{g}^2 (T_c^2 + T_*^2) v^2 < (1 + c^{-2}) \tilde{g}^2 T_*^2 v^2. \quad (31)$$

Thus, the parameter α scales in this limit as

$$\alpha \propto \frac{\Delta V}{T_*^4} \propto \frac{1}{\Delta V} \propto \frac{1}{T_*^2}. \quad (32)$$

Moreover, small latent heat ϵ_* and thus small $|\Delta V(0)|$ tend to increase the three-dimensional tunnel action

$$140 T_* \approx S_3(T_*) \propto \Delta V(T_*)^{-2} > \Delta V(0)^{-2}, \quad (33)$$

such that the condition in Eq. (A13) implies that large α not only requires a small $|\Delta V(0)|$, but also a very small potential well between the two minima. Our numerical analysis indicates that this seems not to be compatible with the mass constraints on the charginos and Higgs bosons in the nMSSM, what limits the strength of the phase transition. Nevertheless, with further tuning a somewhat larger value for α might be possible.

VI. ELECTROWEAK BARYOGENESIS

While the plasma is driven out of equilibrium by the expansion of the Higgs bubbles during the phase transition, CP violation is provided by the complex coefficients in the potential of Eq. (20). After redefinition of the fields, all sources of CP violation can be attributed solely to the parameter t_s by a complex phase. (We do not consider a CP-violating phase in the Wino mass, as was done in Ref. [21].) As mentioned before, the nMSSM does not contain an explicit Higgsino mass μ , but only an induced Higgsino mass from the singlet-Higgs coupling according to

$$\mu = \lambda \langle S \rangle. \quad (34)$$

The change in the complex phase of the singlet during the phase transition gives rise to a CP-violating current of charginos in the bubble wall. Via Yukawa interactions, this CP

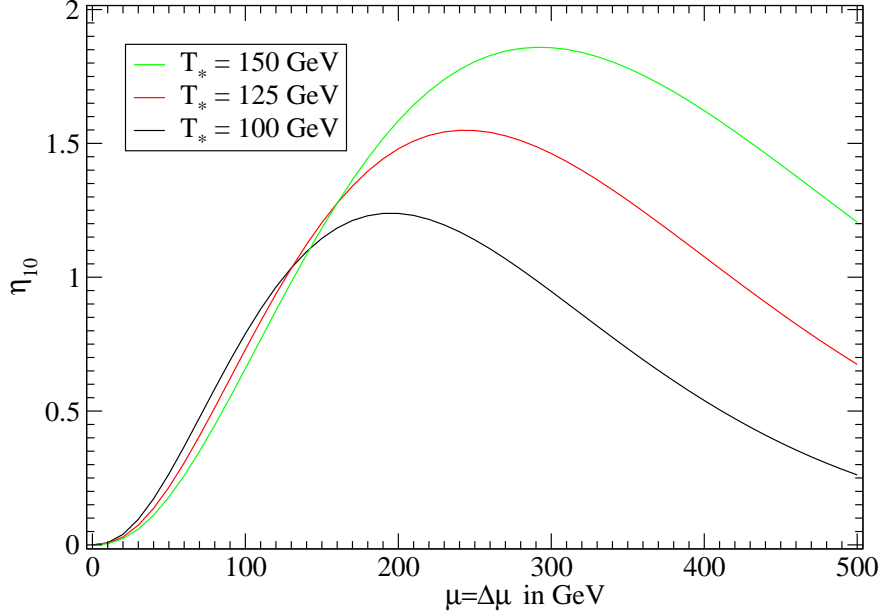


FIG. 7: The baryon asymmetry η_{10} for different critical temperatures T_* , $\Delta\text{Arg}(\mu) = \pi/10$ and $l_w T_* = 10$.

violation is communicated to the tops that bias the sphaleron process. This mechanism is called chargino mediated electroweak baryogenesis and was analyzed in the MSSM in Refs. [33, 34, 35, 36]. The formalism we use to determine the BAU was developed in the series of papers [36] and recently applied to the nMSSM [22].

In the case of a large Wino mass parameter, $M_2 \gtrsim 1$ TeV, the change in the complex phase, $\Delta\text{Arg}(\mu)$, during the phase transition is the main source of baryon number generation and a good estimate of the predicted η_{10} is given by

$$\eta_{10} \approx c(T_*) \frac{\Delta\text{Arg}(\mu)}{\pi} \frac{1}{l_w T_*} \left(\frac{\mu_0}{\tau T_*} \right)^{\frac{3}{2}} \frac{\Delta\mu}{\tau T_*} \exp(-\mu_0/\tau T_*), \quad (35)$$

where μ_0 denotes the μ parameter in the symmetric phase, $\Delta\mu$ the change in μ during the phase transition and l_w the thickness of the bubble wall. The two coefficients are $c(T_*) \approx 1.6 T_*/\text{GeV}$ and $\tau \approx 0.78$. The function η_{10} is plotted in Fig. 7 for $\mu = \Delta\mu$ and several values of T_* and shows very good agreement with the full numerical results of the diffusion equations given in Ref. [22]. Under these assumptions, electroweak baryogenesis is a quite generic feature of the nMSSM. In the present case, these results are not directly applicable, since they have been obtained using a wall velocity smaller than the speed of sound. In this regime, the produced BAU does not strongly depend on the precise velocity

of the wall. For not too strong phase transitions, subsonic bubble velocities are motivated by calculations of the friction effects acting on the bubble wall [37, 38].

On the other hand, as has been explained earlier, for an observable production of GWs, wall velocities beyond the speed of sound are necessary. This is problematic for standard electroweak baryogenesis, since in this regime diffusion processes are strongly suppressed. However, even if the analysis based on diffusion is not valid, other mechanisms, as e.g. quantum mechanical reflection at the wall [39] might be responsible for the production of the baryon asymmetry. The relevant parameters that enter a quantitative analysis of the produced BAU are in fact similar. For example, in the case of the nMSSM with a very strong phase transition, one would expect that the produced baryon asymmetry is small since the low temperature leads to Boltzmann suppressed chargino densities. This problem might be avoided in scenarios where the CP violation is supplied by SM particles that are massless in the symmetric phase, as e.g. in the model with dimension-six operators discussed in Ref. [26, 27]. Nevertheless, a strongly first-order phase transition with supersonic bubble velocities seems to disfavor baryon production at the electroweak scale.

VII. CONCLUSIONS

In conclusion, we found that the density of GWs produced during a strongly first-order electroweak phase transition is in a large portion of parameter space too small to be detectable by LISA or even the BBO experiment, both for the nMSSM and the Standard Model with dimension-six operators. This is partially because stronger phase transitions proceed at lower temperatures and create larger bubbles, which shifts the peak of the spectrum of the GW density to lower frequencies. This correlation was not taken into account in the model independent analysis of Ref. [16], which therefore led to more optimistic conclusions. For the nMSSM our results are best summarized by Fig. 6 which displays the spectrum of GW densities for several parameter sets, and for the Standard Model with dimension-six operators by Fig. 2. Moreover, we observe that very strong phase transitions, $\alpha > 0.2$, in the nMSSM are not compatible with constraints on the particle spectrum, or at least require a significant amount of tuning. The situation in the Standard Model with dimension-six operators is slightly more promising. Besides, it is easier to understand the effects of parameter tuning in this case. Generating observable GWs at BBO requires a few

percent tuning in the suppression scale of the dimension-six operator.

Technically, our main improvement was the full numerical computation of the bubble configurations, which leads to more realistic predictions on the properties of the phase transition that enter the GW computation. The simple approximation to bubble profiles in Ref. [17] seems to considerably overestimate the strength of the phase transition and in turn the GW signal.

On electroweak scales, a strongly first-order phase transition is a necessary prerequisite for electroweak baryogenesis as well as for sizable GW production. However, there is no positive correlation between GW observations and electroweak baryogenesis. In the nMSSM, for all parameter sets under consideration, washout is suppressed after the phase transition and electroweak baryogenesis might be possible. Besides, GW production is marginal for many parameter sets, such that electroweak baryogenesis cannot be excluded, even if GWs are not observed down to a sensitivity of $h_0^2\Omega = 10^{-20}$. On the other hand, observing GWs in the near future does not directly support electroweak baryogenesis. In fact, the opposite might be true. Since significant GW production by collisions and turbulence requires supersonic bubble wall expansion, diffusion is suppressed which reduces the produced BAU in mechanisms based on transport. Due to rather thin walls, other mechanisms, as e.g. CP-violating reflection, might be effective in this regime, but reliable predictions in this scenario are missing. Additionally, in the case of the nMSSM, observable GW production is only possible (if at all) for small critical temperatures, what further reduces the prospects of chargino mediated baryogenesis due to Boltzmann suppressed chargino densities, even if they are not based on transport.

Hence, the observation of GWs that can be attributed to the electroweak phase transition, could not only partially shadow a smoking gun signal from inflation, but also question (at least the standard picture of) electroweak baryogenesis.

It would be interesting to study baryogenesis with supersonic bubbles in more detail. After all, supersonic walls could appear in a larger part of the nMSSM parameter space. Finally, one should keep in mind that especially the turbulence contribution to the GW spectrum is still under debate. The available computations are based on non-relativistic models of turbulence. A numerical simulation of relativistic turbulence would be desirable to obtain more reliable predictions.

Acknowledgments

T.K. is supported by the Swedish Research Council (Vetenskapsrådet), Contract No. 621-2001-1611.

APPENDIX A: THE PHASE TRANSITION

If the two minima of the effective potential are separated by a potential well, thermal and quantum fluctuations lead to small regions in space that acquire a finite Higgs vev close to the global minimum of the effective potential. If this region reaches a critical size, it is advantageous to expand this region, since the gain in energy by increasing the size of the bubble dominates over the increase in energy in the surface of the bubble. The phase transition proceeds then by nucleation and expansion of bubbles consisting of regions with non-vanishing Higgs vev.

In the semi-classical theory of tunneling [40, 41], the tunnel probability depends on the action of the so-called bounce solution. This configuration fulfills the boundary conditions (φ_- denotes the symmetric minimum of the potential $V(\varphi, T)$)

$$\partial_\varrho \varphi(0) = 0, \quad \lim_{\varrho \rightarrow \infty} \varphi(\varrho) = \varphi_- \quad (\text{A1})$$

and the Euclidean equation of motion

$$\frac{\partial^2 \varphi}{\partial \varrho^2} + \frac{\gamma}{\varrho} \frac{\partial \varphi}{\partial \varrho} = V'(\varphi), \quad (\text{A2})$$

and $\gamma = 2(3)$ corresponds to tunneling at finite temperature (in vacuum). At finite temperature, the bubble nucleation rate is then given by

$$\Gamma = A T^4 e^{-S_3/T}, \quad (\text{A3})$$

where A is a constant of $\mathcal{O}(1)$ and the Euclidean action is

$$S_3 = 4\pi \int dr r^2 \left[\frac{1}{2} \left(\frac{d\varphi}{dr} \right)^2 + V(\varphi, T) \right]. \quad (\text{A4})$$

To determine the bounce configuration, we use the method presented in Ref. [19]. This method is based on a two step procedure. First, the bounce solution is determined without damping, $\gamma = 0$, which can be achieved relatively simple due to energy conservation. Subsequently, the parameter γ is continuously increased to the desired value, $\gamma = 2$, while a linearized version of the discretized equation of motion is iteratively solved.

The temperature when the phase transition occurs depends besides the Euclidean action $S_3(T)$ on the cosmological parameters [5]. The expansion of the Universe is characterized by the Hubble parameter

$$H^{-1} = \frac{2\xi M_{pl}}{T^2}, \quad (\text{A5})$$

where $M_{pl} = 1.22 \times 10^{19}$ GeV denotes the Planck mass, and near the electroweak phase transition $\xi \simeq 1/34$. The probability that a bubble was nucleated inside the causal volume is given by

$$dP = A \frac{T^4}{H^4} e^{-S_3/T} \frac{dT}{T}. \quad (\text{A6})$$

The temperature of the beginning of the phase transition T_n is defined by the nucleation of the first bubble

$$P|_{T=T_n} = \int_{T_n}^{\infty} dP = 1. \quad (\text{A7})$$

On the other hand, most gravitational radiation is emitted at the end of the phase transition when the bubbles collide. Neglecting the expansion of the Universe, the radius of a bubble at the temperature T_x that nucleated at temperature T and expands with a velocity v_b is given by [5]

$$R(T_x, T) = v_b \frac{T_x}{H(T_x)} \left(\frac{1}{T_x} - \frac{1}{T} \right). \quad (\text{A8})$$

Thus, the fraction of the causal volume that is in the broken phase is

$$f(T_x) \simeq \frac{4\pi H^3}{3} \int_{T_x}^{\infty} R^3(T_x, T) dP. \quad (\text{A9})$$

We define the end of the phase transition to be given by

$$f|_{T_x=T_f} = 1. \quad (\text{A10})$$

Another relevant quantity in the analysis of gravitational wave production is the typical size of the nucleated bubbles at the end of the phase transition, $\langle R \rangle$. Following Ref. [15], we use the maximum of the bubble volume distribution, $dV \propto R^3 dP$, which should be closely related to the typical scale for energy injection into the turbulent plasma. In this case, one obtains the condition (see Eqs. (3) and (A8))

$$\langle R \rangle \approx 3 \frac{v_b}{\beta(T_R)}, \quad T_R = \frac{v_b T_f}{v_b - H(T_f) \langle R \rangle}. \quad (\text{A11})$$

This definition has the virtue that it characterizes typical bubble sizes at the end of the phase transition in a reasonable way, even for very strong phase transitions, in contrast to $\beta(T_f)$ that even can become negative.

Finally, N is the number of bubbles per causal volume at the end of the phase transition

$$N = P|_{T=T_f}. \quad (\text{A12})$$

To obtain approximate results for these quantities, a Taylor expansion of the action can be used. Performing the integrals in Eqs. (A7), (A9) and (A12) leads to

$$\left. \frac{S_3}{T} \right|_{T=T_n} \approx 141.4 - 4 \log \left(\frac{T_n}{100 \text{GeV}} \right) - \log \left(\frac{\beta(T_n)}{100} \right), \quad (\text{A13})$$

$$\left. \frac{S_3}{T} \right|_{T=T_f} \approx 130.8 - 4 \log \left(\frac{T_f}{100 \text{GeV}} \right) - 4 \log \left(\frac{\beta(T_f)}{100} \right) + 3 \log v_b, \quad (\text{A14})$$

$$N|_{T=T_f} \approx \left. \frac{1}{8\pi} \left(\frac{\beta}{v_b H} \right)^3 \right|_{T=T_f}. \quad (\text{A15})$$

- [1] M. S. Turner, “Detectability of inflation-produced gravitational waves,” *Phys. Rev. D* **55** (1997) 435 [arXiv:astro-ph/9607066].
- [2] K. Danzmann and A. Rudiger, “Lisa Technology - Concept, Status, Prospects,” *Class. Quant. Grav.* **20** (2003) S1.
- [3] V. Corbin and N. J. Cornish, “Detecting the cosmic gravitational wave background with the big bang observer,” *Class. Quant. Grav.* **23** (2006) 2435 [arXiv:gr-qc/0512039].
G. M. Harry, P. Fritschel, D. A. Shaddock, W. Folkner and E. S. Phinney, “Laser Interferometry For The Big Bang Observer,” *Class. Quant. Grav.* **23** (2006) 4887.
- [4] V. A. Kuzmin, V. A. Rubakov and M. E. Shaposhnikov, “On The Anomalous Electroweak Baryon Number Nonconservation In The Early Universe,” *Phys. Lett. B* **155**, 36 (1985).
- [5] G. W. Anderson and L. J. Hall, “The Electroweak Phase Transition And Baryogenesis,” *Phys. Rev. D* **45** (1992) 2685.
- [6] A. Kosowsky, M. S. Turner and R. Watkins, “Gravitational Radiation From Colliding Vacuum Bubbles,” *Phys. Rev. D* **45** (1992) 4514.
- [7] A. Kosowsky, M. S. Turner and R. Watkins, “Gravitational waves from first order cosmological phase transitions,” *Phys. Rev. Lett.* **69** (1992) 2026.
- [8] A. Kosowsky and M. S. Turner, “Gravitational Radiation From Colliding Vacuum Bubbles: Envelope Approximation To Many Bubble Collisions,” *Phys. Rev. D* **47** (1993) 4372 [arXiv:astro-ph/9211004].

- [9] M. Kamionkowski, A. Kosowsky and M. S. Turner, “Gravitational radiation from first order phase transitions,” *Phys. Rev. D* **49**, 2837 (1994) [arXiv:astro-ph/9310044].
- [10] A. Kosowsky, A. Mack and T. Kahniashvili, “Stochastic gravitational radiation from phase transitions,” arXiv:astro-ph/0102169.
- [11] A. Kosowsky, A. Mack and T. Kahniashvili, “Gravitational radiation from cosmological turbulence,” *Phys. Rev. D* **66**, 024030 (2002) [arXiv:astro-ph/0111483].
- [12] A. D. Dolgov, D. Grasso and A. Nicolis, “Relic backgrounds of gravitational waves from cosmic turbulence,” *Phys. Rev. D* **66**, 103505 (2002) [arXiv:astro-ph/0206461].
- [13] C. Caprini and R. Durrer, “Gravitational waves from stochastic relativistic sources: Primordial turbulence and magnetic fields,” *Phys. Rev. D* **74** (2006) 063521 [arXiv:astro-ph/0603476].
- [14] G. Gogoberidze, T. Kahniashvili and A. Kosowsky, “The spectrum of gravitational radiation from primordial turbulence,” arXiv:0705.1733 [astro-ph].
- [15] A. Nicolis, “Relic gravitational waves from colliding bubbles and cosmic turbulence,” *Class. Quant. Grav.* **21** (2004) L27 [arXiv:gr-qc/0303084].
- [16] C. Grojean and G. Servant, “Gravitational waves from phase transitions at the electroweak scale and beyond,” *Phys. Rev. D* **75** (2007) 043507 [arXiv:hep-ph/0607107].
- [17] R. Apreda, M. Maggiore, A. Nicolis and A. Riotto, “Gravitational waves from electroweak phase transitions,” *Nucl. Phys. B* **631** (2002) 342 [arXiv:gr-qc/0107033].
- [18] M. Pietroni, “The Electroweak phase transition in a nonminimal supersymmetric model,” *Nucl. Phys. B* **402**, 27 (1993) [arXiv:hep-ph/9207227].
- A. T. Davies, C. D. Froggatt and R. G. Moorhouse, “Electroweak Baryogenesis in the Next to Minimal Supersymmetric Model,” *Phys. Lett. B* **372**, 88 (1996) [arXiv:hep-ph/9603388].
- S. J. Huber and M. G. Schmidt, “SUSY variants of the electroweak phase transition,” *Eur. Phys. J. C* **10**, 473 (1999) [arXiv:hep-ph/9809506].
- S. J. Huber and M. G. Schmidt, “Electroweak baryogenesis: Concrete in a SUSY model with a gauge singlet,” *Nucl. Phys. B* **606**, 183 (2001) [arXiv:hep-ph/0003122].
- M. Bastero-Gil, C. Hugonie, S. F. King, D. P. Roy and S. Vempati, “Does LEP prefer the NMSSM?,” *Phys. Lett. B* **489**, 359 (2000) [arXiv:hep-ph/0006198].
- [19] T. Konstandin and S. J. Huber, “Numerical approach to multi dimensional phase transitions,” *JCAP* **0606**, 021 (2006) [arXiv:hep-ph/0603081].
- [20] C. Panagiotakopoulos and K. Tamvakis, “New minimal extension of MSSM,” *Phys. Lett. B*

- 469**, 145 (1999) [arXiv:hep-ph/9908351].
- C. Panagiotakopoulos and A. Pilaftsis, “Higgs scalars in the minimal non-minimal supersymmetric standard model,” *Phys. Rev. D* **63**, 055003 (2001) [arXiv:hep-ph/0008268].
- [21] A. Menon, D. E. Morrissey and C. E. M. Wagner, “Electroweak baryogenesis and dark matter in the nMSSM,” *Phys. Rev. D* **70** (2004) 035005 [arXiv:hep-ph/0404184].
- [22] S. J. Huber, T. Konstandin, T. Prokopec and M. G. Schmidt, “Electroweak phase transition and baryogenesis in the nMSSM,” *Nucl. Phys. B* **757**, 172 (2006) [arXiv:hep-ph/0606298].
- [23] C. Balazs, M. S. Carena, A. Freitas and C. E. M. Wagner, “Phenomenology of the nMSSM from colliders to cosmology,” *JHEP* **0706**, 066 (2007) [arXiv:0705.0431 [hep-ph]].
- [24] X. Zhang, “Operators analysis for Higgs potential and cosmological bound on Higgs mass,” *Phys. Rev. D* **47** (1993) 3065 [arXiv:hep-ph/9301277].
- [25] C. Grojean, G. Servant and J. D. Wells, “First-order electroweak phase transition in the standard model with a low cutoff,” *Phys. Rev. D* **71**, 036001 (2005) [arXiv:hep-ph/0407019].
- [26] D. Bodeker, L. Fromme, S. J. Huber and M. Seniuch, “The baryon asymmetry in the standard model with a low cut-off,” *JHEP* **0502**, 026 (2005) [arXiv:hep-ph/0412366].
- [27] L. Fromme and S. J. Huber, “Top transport in electroweak baryogenesis,” *JHEP* **0703**, 049 (2007) [arXiv:hep-ph/0604159].
- [28] S. J. Huber, M. Pospelov and A. Ritz, “Electric dipole moment constraints on minimal electroweak baryogenesis,” *Phys. Rev. D* **75**, 036006 (2007) [arXiv:hep-ph/0610003].
- [29] P. J. Steinhardt, “Relativistic Detonation Waves And Bubble Growth In False Vacuum Decay,” *Phys. Rev. D* **25**, 2074 (1982).
- [30] G. D. Moore, “Measuring the broken phase sphaleron rate nonperturbatively,” *Phys. Rev. D* **59**, 014503 (1999) [arXiv:hep-ph/9805264].
- [31] C. Hugonie, J. C. Romao and A. M. Teixeira, “Spontaneous CP violation in non-minimal supersymmetric models,” *JHEP* **0306** (2003) 020 [arXiv:hep-ph/0304116].
- [32] S. W. Ham, S. K. Oh, C. M. Kim, E. J. Yoo and D. Son, “Electroweak phase transition in a nonminimal supersymmetric model,” *Phys. Rev. D* **70** (2004) 075001 [arXiv:hep-ph/0406062].
- [33] J. M. Cline, M. Joyce and K. Kainulainen, “Supersymmetric electroweak baryogenesis,” *JHEP* **0007** (2000) 018 [arXiv:hep-ph/0006119].
- J. M. Cline, M. Joyce and K. Kainulainen, “Supersymmetric electroweak baryogenesis. (Erratum),” arXiv:hep-ph/0110031.

- [34] M. Carena, J. M. Moreno, M. Quiros, M. Seco and C. E. M. Wagner, “Supersymmetric CP-violating currents and electroweak baryogenesis,” Nucl. Phys. B **599** (2001) 158 [arXiv:hep-ph/0011055].
- [35] M. Carena, M. Quiros, M. Seco and C. E. M. Wagner, “Improved results in supersymmetric electroweak baryogenesis,” Nucl. Phys. B **650** (2003) 24 [arXiv:hep-ph/0208043].
- [36] T. Konstandin, T. Prokopec and M. G. Schmidt, “Kinetic description of fermion flavor mixing and CP-violating sources for baryogenesis,” Nucl. Phys. B **716**, 373 (2005) [arXiv:hep-ph/0410135].
T. Konstandin, T. Prokopec, M. G. Schmidt and M. Seco, “MSSM electroweak baryogenesis and flavour mixing in transport equations,” Nucl. Phys. B **738**, 1 (2006) [arXiv:hep-ph/0505103].
- [37] G. D. Moore and T. Prokopec, “How fast can the wall move? A Study of the electroweak phase transition dynamics,” Phys. Rev. D **52** (1995) 7182 [arXiv:hep-ph/9506475].
- [38] P. John and M. G. Schmidt, “Do stops slow down electroweak bubble walls?,” Nucl. Phys. B **598** (2001) 291 [Erratum-ibid. B **648** (2003) 449] [arXiv:hep-ph/0002050].
- [39] M. E. Shaposhnikov, “Standard Model Solution Of The Baryogenesis Problem,” Phys. Lett. B **277** (1992) 324 [Erratum-ibid. B **282** (1992) 483].
- [40] S. R. Coleman, “The Fate Of The False Vacuum. 1. Semiclassical Theory,” Phys. Rev. D **15** (1977) 2929 [Erratum-ibid. D **16** (1977) 1248].
- [41] A. D. Linde, “Fate Of The False Vacuum At Finite Temperature: Theory And Applications,” Phys. Lett. B **100** (1981) 37.